0.1 A New Joint P and S-wave Mantle Velocity Model for Teleseismic Event Location

Using the insight obtained from performing global location tests using previous generation 3-D models, we recently constructed a new joint P- and S-velocity model of the mantle. To ensure compatibility with regional models which we are also simultaneously constructing, we chose a parameterization of horizontal spherical splines and cubic b-splines in radius (Figure 1). The velocity perturbations are defined by:

$$\delta v(r, \vartheta, \varphi) = \sum_{i,j} C_{ij}\, S_i(\vartheta, \varphi) \cdot B_j(r); \tag{1}$$

where S_i is a spherical spline (Wang and Dahlen, 1995) centered on the coordinates (ϑ_i, φ_i) and $B_j(r)$ is a cubic b-spline centered on the radius r_j. The spline representation is a 'local' description of the model, in contrast to 'global' descriptions, based on spherical harmonics and Chebyshev polynomials, for example. This parameterization easily allows replacement of various portions of the model with more detailed regional models as they become available. The resolution in this model is described by the order of spherical triangles. If $N = 1$ corresponds to 20 equilateral triangles of approximately 63° per side, the spherical spline order N corresponds to the division of a sphere's surface into $20 \cdot N^2$ triangles with $10 \cdot N^2 + 2$ knots. $N = 6$ then corresponds to 362 knots, more or less equivalent to the spherical harmonic expansion to degree 18.

In developing this model, we attempted to further reduce the tradeoff between structure and source locations by relocating the sources in the previous Harvard 3-D model SP12 (Su and Dziewonski, 1993). The P wave data set is adopted from the catalog published by Engdahl *et al.* (1998). After relocation, the travel times were form into summary rays with sources and receivers at the center of 2° x 2° cells. The shallowest layer was 50 km thick and all sources deeper than 50 km were grouped into 100 km thick cells. Events which moved more than 1° from the location published by Engdahl *et al.* (1998) were discarded. In all, the new data set consists of over 626,000 summary rays (Figure 2). The effect of the improvements in the travel time dataset is shown in Figure 3, and it is quite substantial in the shallow mantle. The top panels in Figure 3 show P velocity in the upper mantle from inversion of the new dataset, while the middle panels show model BDP98 (Boschi and Dziewonski, 1999) at the same depths, which used essentially the same data but without the new improvements. The sign of velocity anomalies is the same in both models, but the amplitude of the new model is significantly larger in many areas.

To this travel time dataset, we add the Love and Rayleigh wave dispersion measurements made by Ekström *et al.* (1997) in the period range 35-150 s previously used in the development of a degree-20 spherical harmonic model of S-wave velocity (Ekström and Dziewonski, 1998). The shear velocity model is also constrained by a set of some 50,000 S wave travel times that have been processed in a similar manner as the summary P travel times, as well as an extensive set of differential travel times involving core reflected and refracted shear waves (Ekström, 2000). We are currently adding the capability to use waveforms and complete seismograms in the split b-spline parameterization, which should help to constrain further velocities in the transition zone.

In our inversion, we also attempted to boost resolution in the upper mantle by using as a starting model an S velocity model (Gu *et al.*, 2001) scaled by an appropriate factor. Since it is reasonable to assume that velocity perturbations in the shallow mantle are primarily caused by thermal effects, the assumption that compressional velocity is proportional to shear velocity is likely to be reasonable. We inverted for perturbations to this model using a damping scheme which varies the amount of damping of the size of the model with depth. In other words, more departure from the starting model is allowed in the lower mantle than in the upper mantle.

Figure 4 shows the new global P velocity model at a variety of depths. The amplitude in the shallow mantle is similar to lower resolution models such as SP12 and MK12/WM13 (Su and Dziewonski, 1997) and continental roots appear to extend to 300 km or deeper. This is largely the result of the damping scheme in the upper mantle as these features appear strongly in the starting model. Long, linear high velocity anomalies in the mid-mantle seen in previous models (Grand *et al.*, 1997; van der Hilst *et al.*, 1997) are also seen in the mid-mantle. In the lower mantle we allow the inversion to depart more freely from the starting model and as a result the degree-2 pattern seen in many other models, while still present, is not as strong. The model correlates quite will in the upper mantle with the recent model by Scripps (SB10L18) and with SP12. Both of these models were obtained using other data in addition to travel times. Correlation with models which only use travel times (e.g., Boschi and Dziewonski, 1999; van der Hilst *et al.*, 1997) is lower.

Most importantly, the new model improves location of reference events over all previous global models we have tested. We tested the new model using teleseismic P phases from events listed in the ground-truth database of the Prototype International Data Centre (PIDC), and also the list of reference events compiled in Kennett and Engdahl (1991). Figure 5 shows the mislocations obtained for the new model (P362) versus SP12 for those events having more than 10 teleseismically recoreded P waves. For the explosions in the database, the improvement is quite significant with the average mislocation being reduced by over 15suggests that perhaps the limit of accuracy in the known epicentral parameters has been approached for these events. We find that the direction of mislocation is practically unchanged using the new model.

0.2 Compilation of Reference Events in the Oceans

The second major aspect of our ongoing research concerns the compilation of reference events in regions where local control is lacking, such as mid-ocean ridges. We take advantage of the fact that we know the focal mechanisms for the larger events (through the Harvard CMT catalog) and that ridge segments and transform faults are often sharply defined by the bathymetry. These larger events are selected as "master events" and relocated according to the following process.

First, each master event is associated with a ridge segment or transform fault based on its focal mechanism. Secondly, we rotate the coordinate system to that defined by the plate boundary (i.e., for ridges perpendicular to the spreading direction the ridge defines a parallel or meridian). The location of the plate boundary is defined by features of the bathymetry map (Smith and Sandwell, 1997). Then the location of the event can be confined to a single line, effectively reducing the inversion problem to determination of a single distance.

This technique can also be used in the case of oblique ridges by constraining the ratio of latitude/longitude perturbation. The model used for the location procedure is PREM with corrections for 3-D mantle structure calculated for model SP12.

We have relocated about 1,500 globally distributed events for the period 1977 to 1996, except for some areas where the bathymetry map is too complex or not available (Figure 6). The events move as much as 50 km from the initial location provided by the ISC (Figure 7). Such large location shifts, if real, are likely to have a significant effect on velocity structure in the upper mantle recovered in tomographic inversions. When the database of new reference events becomes sufficiently large, we plan to incorporate it into our inversions for mantle structure, and also into our ongoing determination of surface wave phase velocities. In addition, we believe that it is possible to further expand the coverage of this dataset by making use of currently available 2-minute gravity maps. Although the quality of the locations are currently under testing, the residuals with respect to PREM are often smaller for the relocated epicenter than for the initial ISC location.

For smaller events in the oceans, for which a focal mechanism has not been determined, it is possible to use a Joint Hypocentral Determination technique in conjunction with a nearby master event (one already located using the above procedure). For this procedure, we propose to incorporate all events with sufficient phase readings within 50 km of a master event, and invert simultaneously for corrections to the epicentral parameters and for station corrections (Pan *et al.*, 2000). Figure 8 shows JHD location of a cluster of events relative to a new master event along the Romanche Fracture Zone. It may thus be possible to develop almost a continuously distributed set of test events in the remote oceans for calibration purposes. Since published locations in these regions are known to contain large errors, this database may be of considerable use even if the relocated epicenters are accurate only to within 10 km.

References

Boschi, L., and A. M. Dziewonski, High and low-resolution images of the Earth's mantle: Implications of different approaches to tomographic modeling ,*J. Geophys. Res., 104*, 25,567-25,594, 1999.

Ekström, G., Mapping the lithosphere and asthenosphere with surface waves: Lateral structure and anisotropy, in *History and Dynamics of Global Plate Motions*, M. A. Richards, R. G. Gordon, and R. D. van der Hilst, eds., American Geophysical Union, Washington, D. C., 2000.

Ekström, G., and A. M. Dziewonski, The unique anisotropy of the Pacific upper mantle, *Nature, 394*, 168-172,1998.

Ekström, G., J. Tromp, and E. W. F. Larson, Measurements and global models of surface wave propagation, *J. Geophys. Res., 102* ,8137-8157, 1997.

Engdahl, E. R., R. D. van der Hilst, and R. P. Buland, Global teleseismic earthquake relocation with improved travel times and procedures for depth determination, *Bull. Seism. Soc. Am., 88*, 722-743, 1998.

Grand, S. P., R. D. van der Hilst, and S. Widiyantoro, Global seismic tomography: A snapshot of convection in the Earth, *GSA Today, 7*(4), 1-7, 1997.

Gu, Y. J., A. M. Dziewonski, W. Su, and G. Ekström, Shear velocity model in the mantle and discontinuities in the pattern of lateral heterogeneities, *J. Geophys. Res.*, in press, 2001.

Kennett, B. L. N., and E. R. Engdahl, Traveltimes for global earthquake location and phase identification, *Geophys. J. Int., 105*, 429–465, 1991.

Pan, J., M. Antolik, and A. M. Dziewonski, Locations of mid-oceanic earthquakes constrained by seafloor bathymetry, EOS, Trans. Am. Geophys. Soc. (supplement), 81, F8682000.

Smith, W. H. F., and D. T. Sandwell, Global sea floor topography from satellite altimetry and ship depth soundings, *Science, 277*, 1956-1962, 1997.

Su, W., and A. M. Dziewonski, Joint 3-D inversion for P- and S-velocity in the mantle, *EOS, Trans. Am. Geophys. Un., 74*, 557, 1993.

Su, W., and A. M. Dziewonski, Simultaneous inversion for 3-D variations in shear and bulk sound velocity in the mantle, *Phys. Earth Planet. Int., 100*, 6,945-6,980, 1997.

van der Hilst, R. D., S. Widiyantoro, and E. R. Engdahl, Evidence for deep mantle circulation from global tomography, *Nature, 386*, , 578-584, 1997.

Wang, Z., and F. A. Dahlen, Spherical-spline parameterization of three-dimensional Earth models, *Geophys. Res. Lett., 22*, 3099-3102, 1995.

Figure 1: Horizontal and radial parameterization of new global joint P and S velocity model. (Top) Lateral distribution of spherical spline knots. (Bottom) Radial distribution of cubic b-splines. Splines are split at the 670 km discontinuity.

Figure 2: Ray coverage in the new summary travel time data set. Number of rays crossing 5° equal-area blocks in 15 layers from the moho to the CMB is shown.

Figure 3: P wave velocity at two depths in the upper mantle. Top panels show results of inversion using only the new improved dataset of summary travel times, while the middle panels display model BDP98 (obtained using an older travel time dataset). The bottom panels show the difference between the two models.

Figure 4: Views of the new global model of P wave velocity at various depths.

Figure 5: Plot of mislocation for global reference events obtained using teleseismic P waves and models SP12 and P362.

Figure 6: Map of master events on mid-ocean ridges relocated using the new technique.

Figure 7: Relocation of master events along the Romanche Fracture Zone and adjacent ridge segments in the central Atlantic. (Top) CMT focal mechanisms for the events. (Bottom) Relocated epicenters (red dots) and vectors pointing to the initial location. Distance scale for the vectors is shown.

Figure 8: Example of JHD relocation of smaller earthquakes with respect to a new master event (large diamond) along the Romanche Fracture Zone. After relocation, the cluster of seismicity is tighter and more linear.

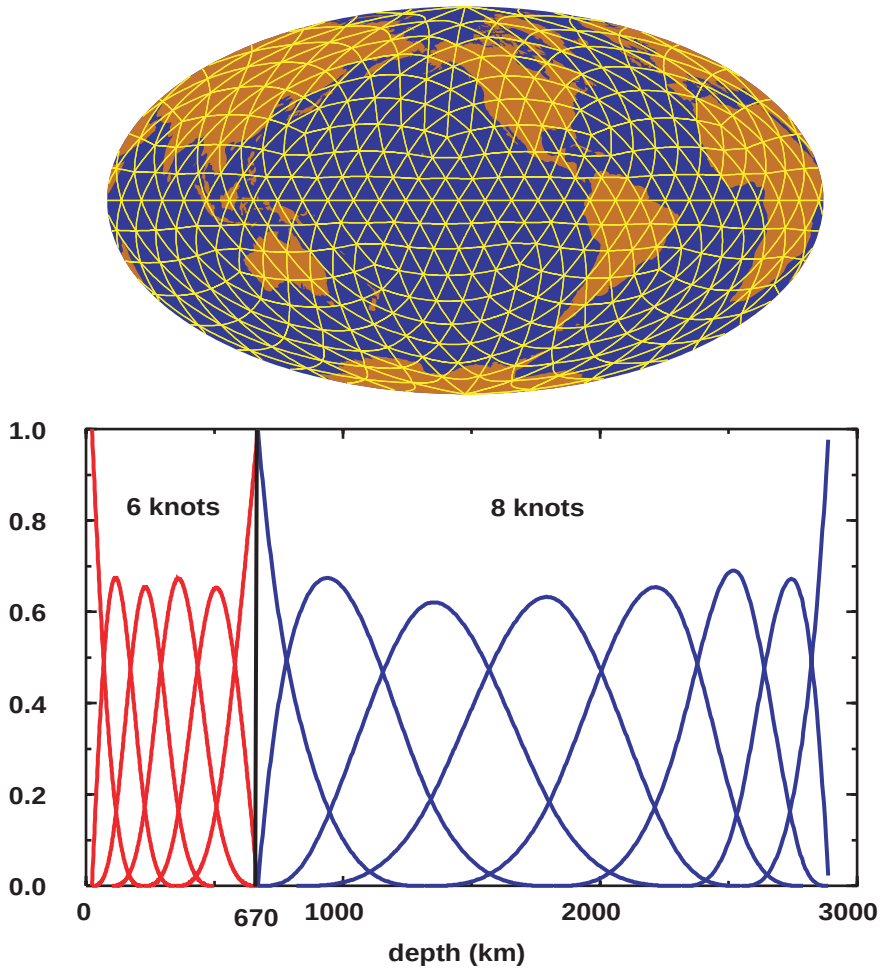
1.0
0.8
0.6
0.4
0.2
0.0
6 knots
8 knots
0
670
1000
2000
3000
depth (km)

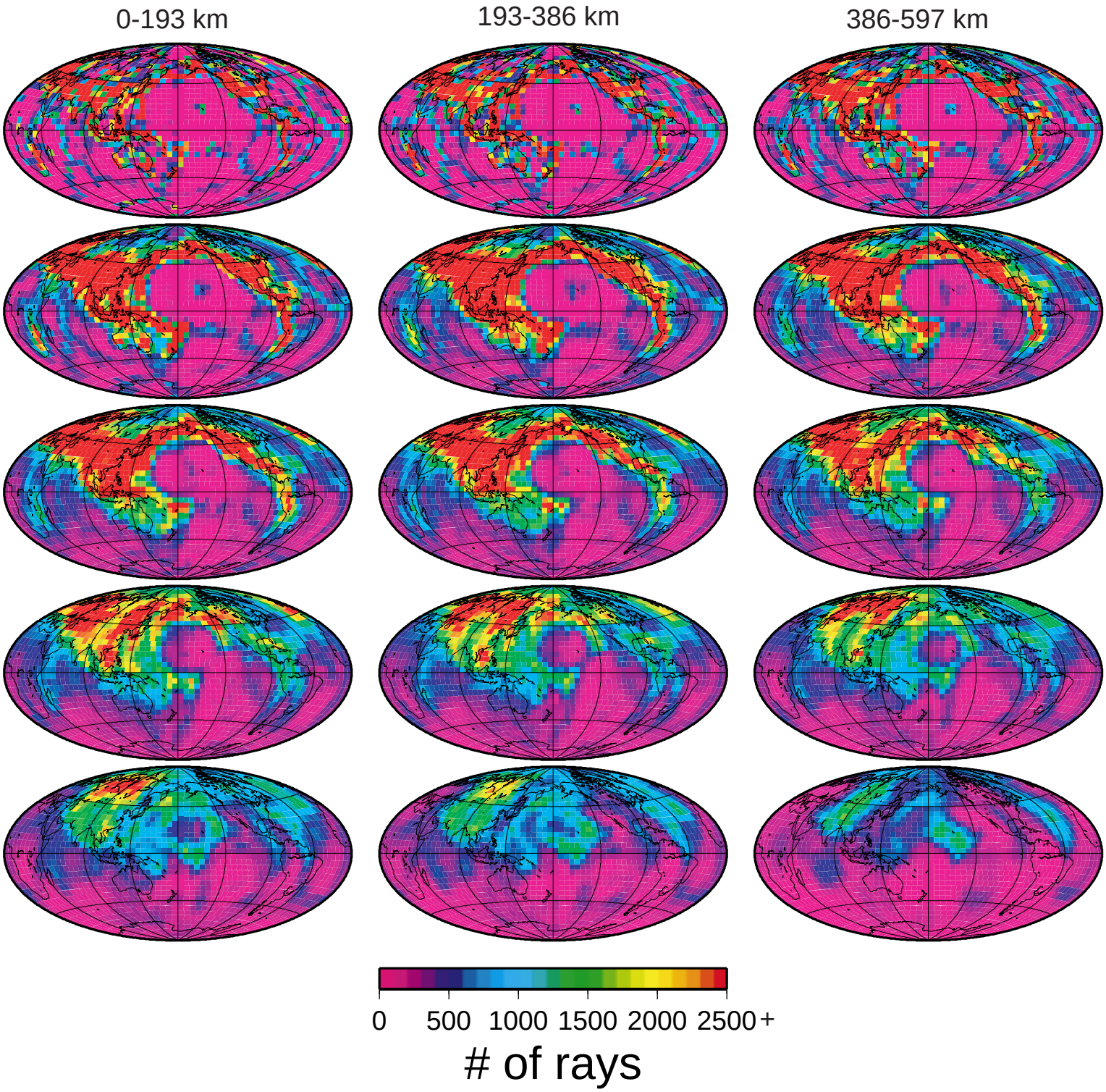
0-193 km
193-386 km
386-597 km
0
500
1000
1500
2000
2500+
# of rays

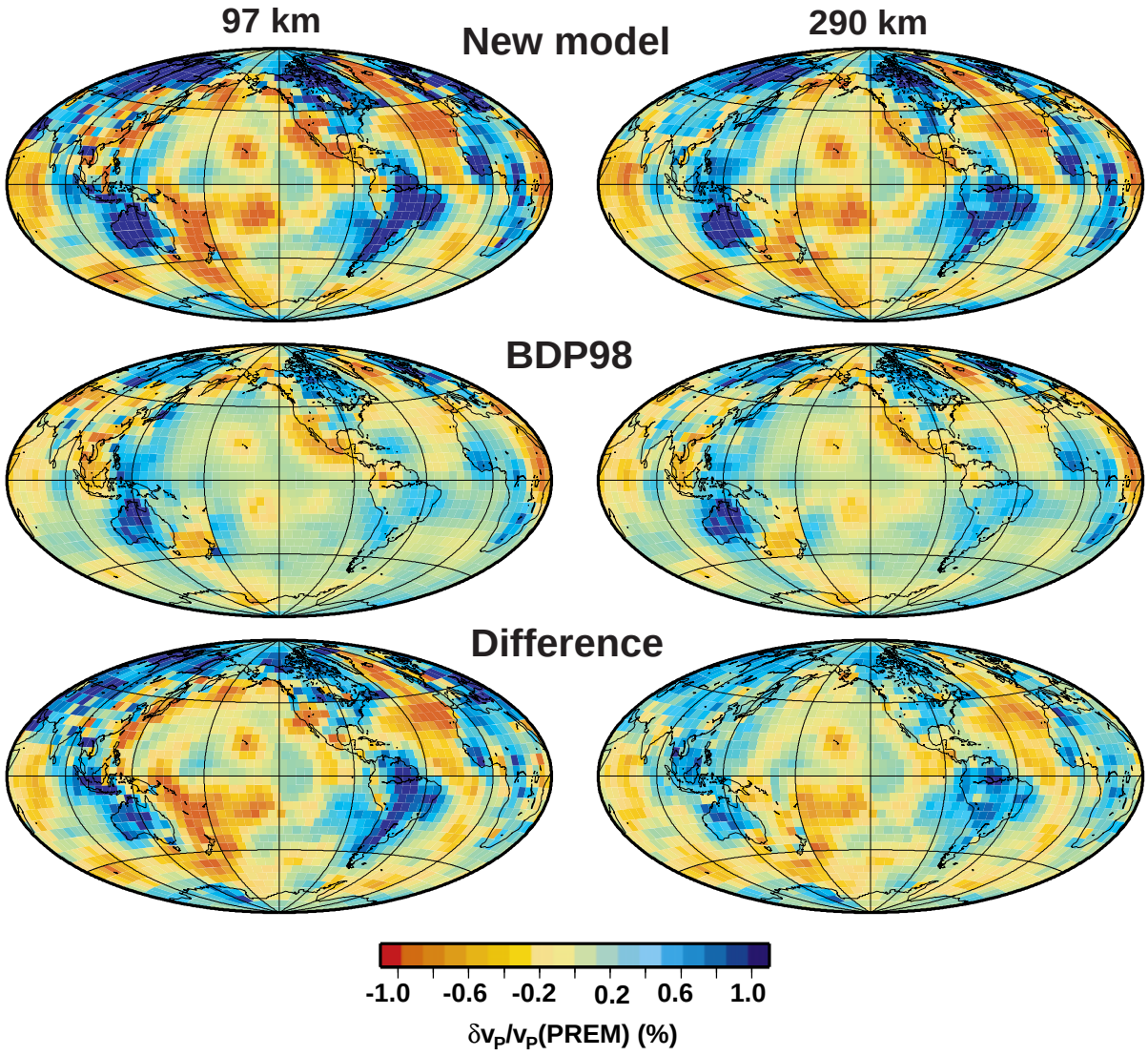
97 km
New model
290 km
BDP98
Difference
-1.0
-0.6
-0.2
0.2
0.6
1.0
δv_P/v_P(PREM) (%)

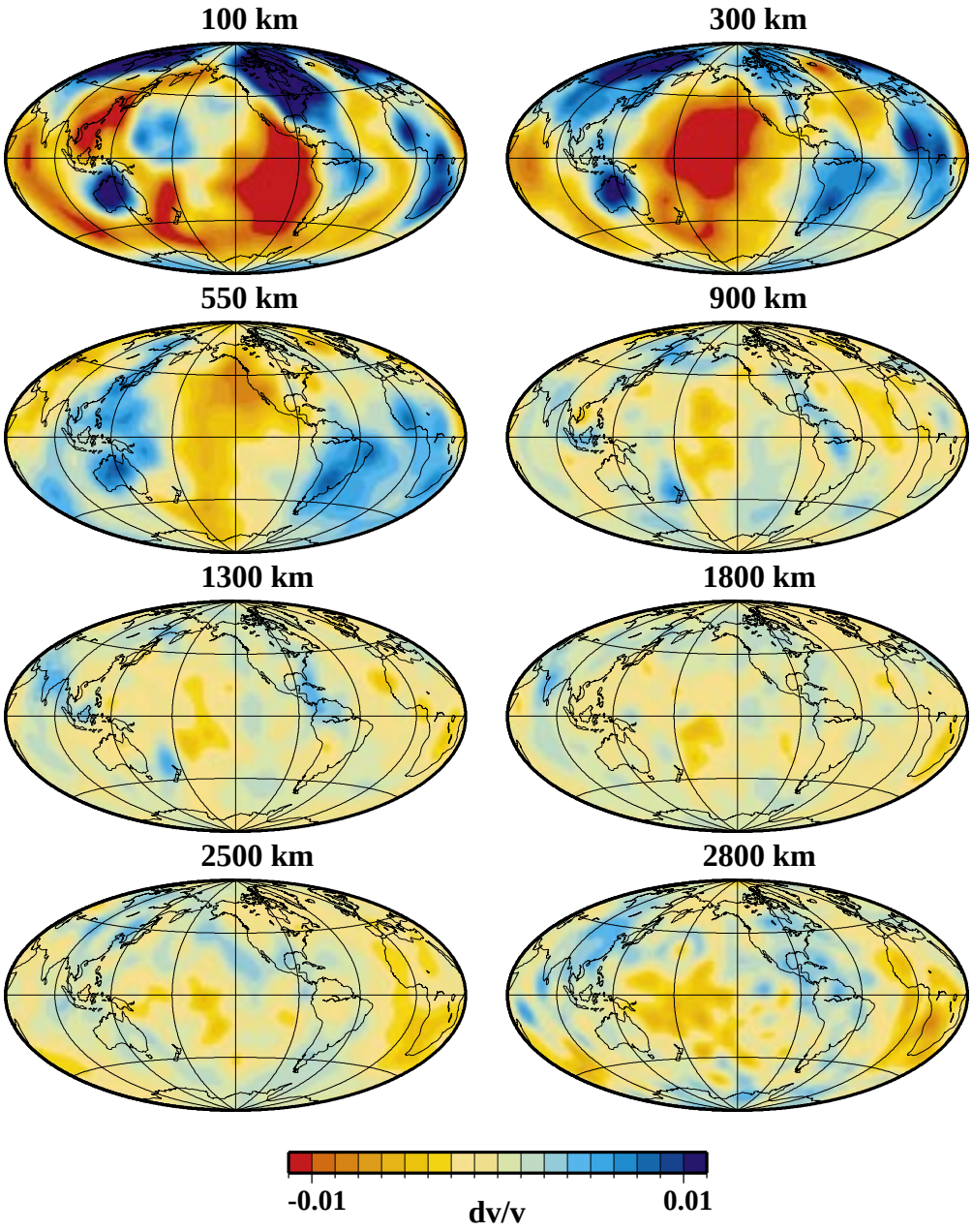
100 km
300 km
550 km
900 km
1300 km
1800 km
2500 km
2800 km
-0.01
dv/v
0.01

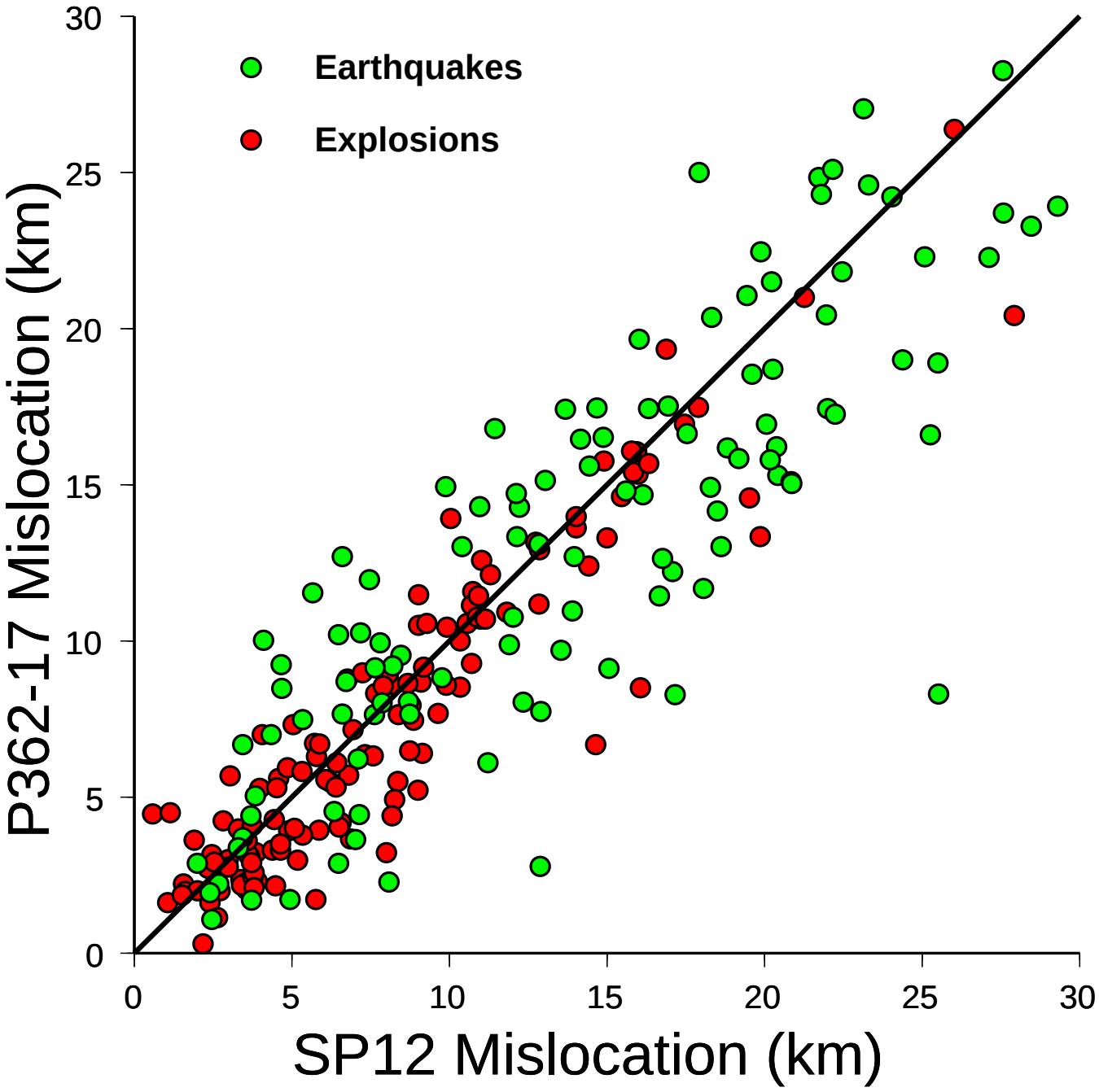
Earthquakes
Explosions
P362-17 Mislocation (km)
SP12 Mislocation (km)
0
5
10
15
20
25
30

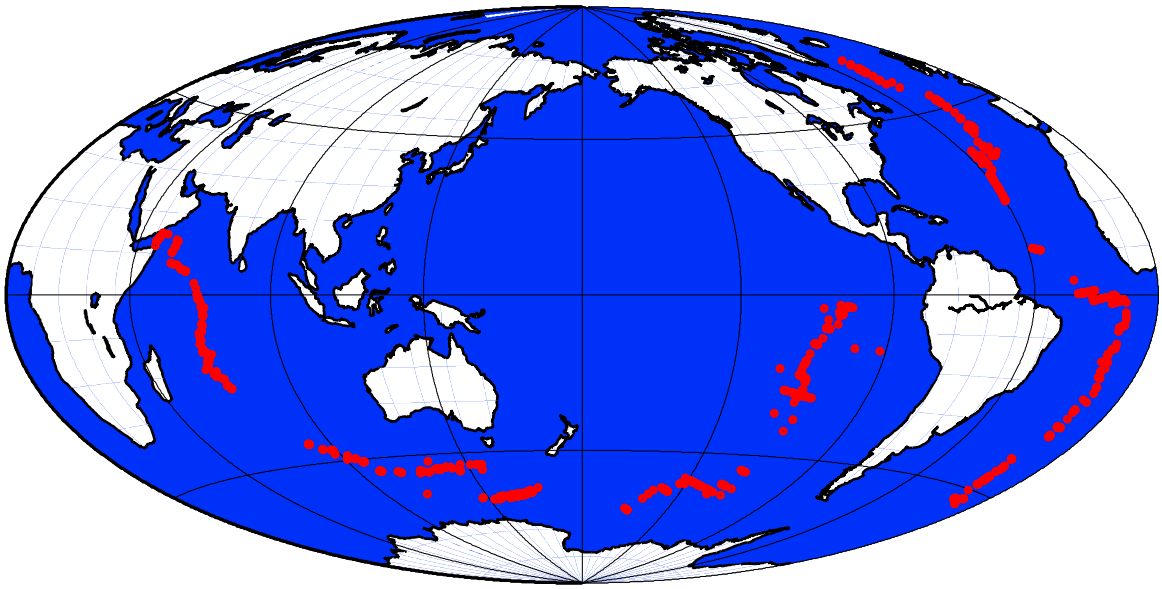

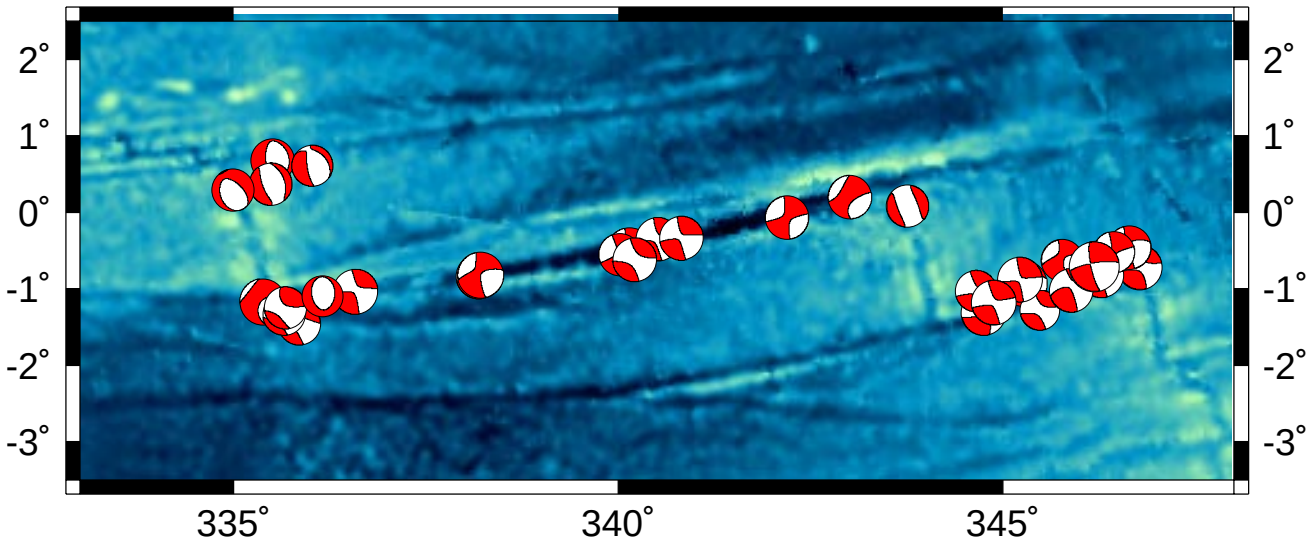
2°
1°
0°
-1°
-2°
-3°
335°
340°
345°

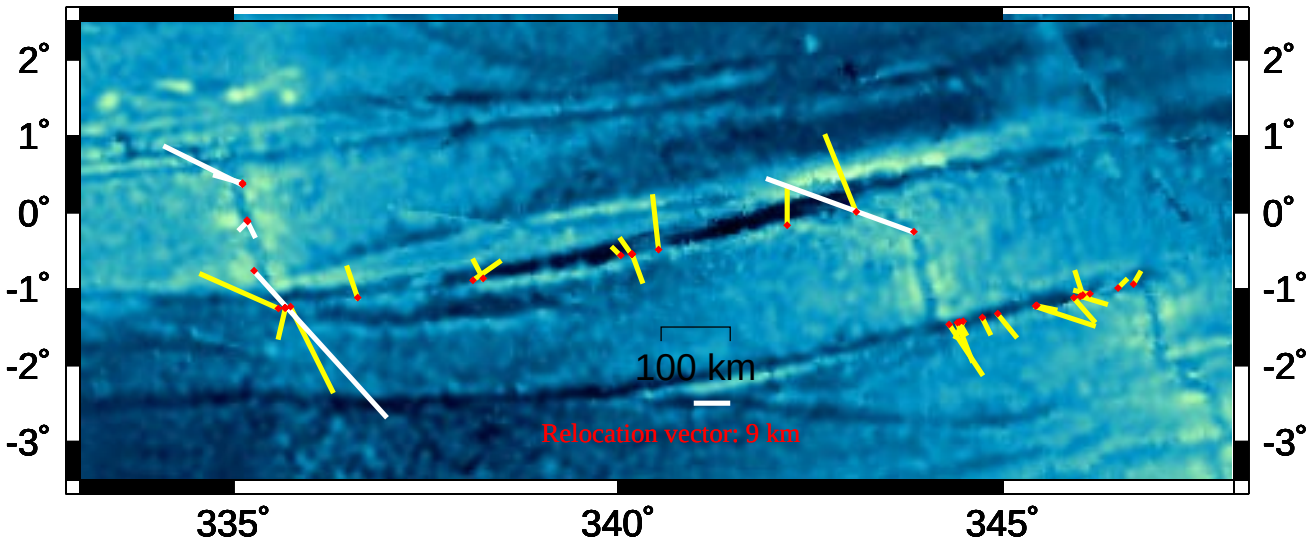
2°
1°
0°
-1°
-2°
-3°
335°
340°
345°
100 km
Relocation vector: 9 km

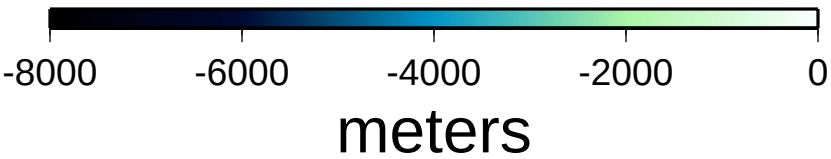
-8000
-6000
-4000
-2000
0
meters

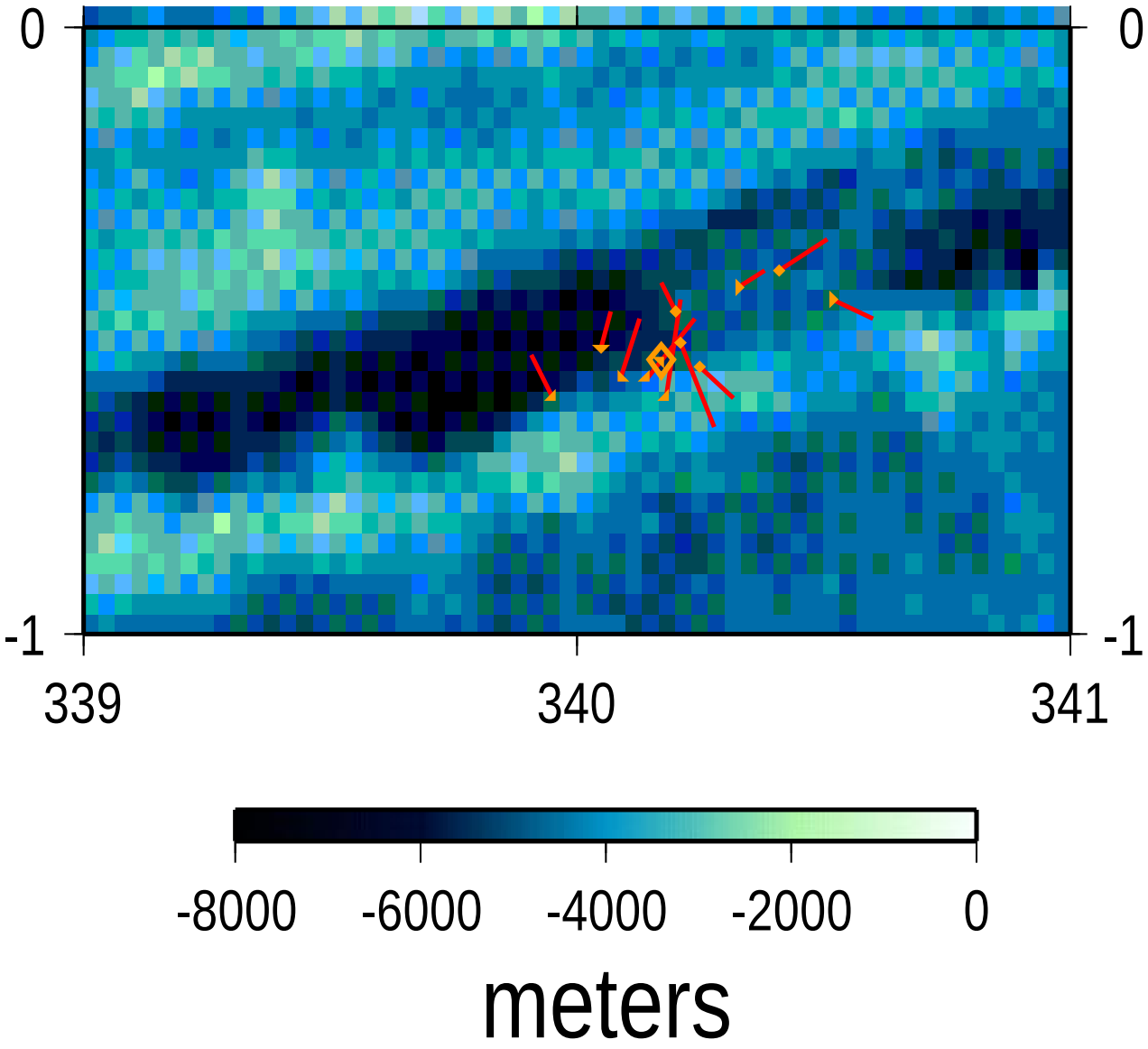
0
0
-1
-1
339
340
341
-8000
-6000
-4000
-2000
0
meters